Nagai, K. (1989) *Nature 336*, 265–266.
Ozaki, Y., Iriyama, K., Ogoshi, H., & Kitagawa, T. (1987) *J. Am. Chem. Soc. 109*, 5583–5586.
Perutz, M. F., Kilmartin, J. V., Nagai, K., Szabo, A., & Simon, S. R. (1976) *Biochemistry 15*, 378–387.
Privalov, P. L., Griko, Yu. V., Venyaminov, S. Yu., & Kutyshenko, V. P. (1986) *J. Mol. Biol. 190*, 487–498.
Puett, D. (1973) *J. Biol. Chem. 248*, 4623–4634.
Reid, L. S., Lim, A. R., & Mauk, A. G. (1986) *J. Am. Chem. Soc. 108*, 8197–8201.
Ringe, D., Petsko, G. A., Kerr, D. E., & Ortiz de Montellano, P. R. (1984) *Biochemistry 23*, 2–4.
Rougee, M., & Brault, D. (1973) *Biochem. Biophys. Res. Commun. 55*, 1364.
Rougee, M., & Brault, D. (1975) *Biochemistry 14*, 4100–4106.
Rousseau, D. L., Ching, Y.-C., Brunori, M., & Giacometti, G. M. (1989) *J. Biol. Chem. 264*, 7878–7881.
Sage, J. T., Morikis, D., & Champion, P. M. (1989) *J. Chem. Phys. 90*, 3015–3032.
Sage, J. T., Li, P., & Champion, P. M. (1991) *Biochemistry* (following paper in this issue).
Sassaroli, M., & Rousseau, D. L. (1987) *Biochemistry 26*, 3092–3098.
Schomacker, K. T., Delaney, J. K., & Champion, P. M. (1986) *J. Chem. Phys. 85*, 4240–4247.
Shelnutt, J. A., Alston, K., Ho, J.-Y., Yu, N.-T., Yamamoto, T., & Rifkind, J. M. (1986) *Biochemistry 25*, 620–627.
Shen, L. L., & Hermans, J., Jr. (1972) *Biochemistry 11*, 1836–1849.
Shimada, H., & Caughey, W. S. (1982) *J. Biol. Chem. 257*, 11893–11900.
Sibbett, S. S., Loehr, T. M., & Hurst, J. K. (1986) *Inorg. Chem. 25*, 307–313.
Spiro, T. G., & Burke, J. M. (1976) *J. Am. Chem. Soc. 98*, 5482–5489.
Šrajer, V., Schomacker, K. T., & Champion, P. M. (1986) *Phys. Rev. Lett. 57*, 1267.
Šrajer, V., Reinisch, L., & Champion, P. M. (1988) *J. Am. Chem. Soc. 110*, 6656–6670.
Tanford, C. (1970) *Adv. Protein Chem. 24*, 1.
Teraoka, J., & Kitagawa, T. (1980) *J. Phys. Chem. 84*, 1928.
Teraoka, J., & Kitagawa, T. (1981) *J. Biol. Chem. 256*, 3969.
Traylor, T. G., Deardurff, L. A., Coletta, M., Ascenzi, P., Antonini, E., & Brunori, M. (1983) *J. Biol. Chem. 258*, 12147–12148.
Traylor, T. G., Koga, N., & Deardurff, L. A. (1985) *J. Am. Chem. Soc. 105*, 6504–6510.
Wang, C.-M., & Brinigar, W. S. (1979) *Biochemistry 18*, 4960–4977.
Warshel, A., & Weiss, R. M. (1981) *J. Am. Chem. Soc. 103*, 446–451.
Yu, N.-T., & Kerr, E. A. (1988) in *Applications of Raman Spectroscopy to Biological Systems* (Spiro, T. G., Ed.) pp 39–95, Wiley, New York.

Spectroscopic Studies of Myoglobin at Low pH: Heme Ligation Kinetics†

J. Timothy Sage, Pusheng Li, and Paul M. Champion*
Department of Physics, Northeastern University, Boston, Massachusetts 02115
Received May 14, 1990; Revised Manuscript Received October 11, 1990

ABSTRACT: On the basis of the characterization of heme structure and ligation in equilibrium, we explore both proximal and distal ligation kinetics of myoglobin below pH 4. Upon photolysis of MbCO, a significant five-coordinate heme population is observed, with an intact iron–histidine bond that persists on the time scale of CO rebinding. Incomplete CO photolysis is attributed to a rapidly exchanging minority population of four-coordinate hemes, which leads to fast ($>10^{10}$ s^{-1}) geminate recombination. The possible relevance of such a mechanism at pH 7 is also noted. Using a novel experimental protocol, we observe the resonance Raman spectrum of partially photolyzed MbCO as a function of continuous wave illumination time (τ). Under extended illumination ($\tau \sim 35$ ms at pH 3.4), there is a loss of intensity in the ν_4 region of the Raman spectrum and the iron–histidine mode is bleached from the spectrum of the five-coordinate photoproduct. In the Fe–CO stretching region of the CO-bound fraction, the intensity of the 526-cm^{-1} mode increases with τ at the expense of the 491-cm^{-1} mode. These changes are interpreted as being due to replacement of the proximal histidine ligand under continuous illumination. Complete relaxation to the pure four-coordinate deoxy heme structure observed in equilibrium is not observed even as $\tau \rightarrow \infty$, presumably since CO rebinding leads to acidification of the iron and its complexation with histidine. We propose a kinetic model to account for our results and discuss the implications for previous low-pH kinetics measurements.

Myoglobin has been widely utilized as a model system for studying the relationship between protein structure, dynamics, and function. Of particular interest is the means by which the protein modulates the rate of binding of small ligands such as CO to the heme. Motion of the iron into the heme plane is believed to make a significant contribution to the activation barrier that must be overcome upon ligand binding. The magnitude of this proximal contribution has been successfully described by a simple harmonic approximation to the iron out-of-plane motion (Šrajer et al., 1988). Distal contributions to ligand binding rates are also likely to be important, and interactions of the bound ligand with the distal histidine are believed to play a key role (Moffat et al., 1979; Doster et al., 1982; Nagai et al., 1987; Olson et al., 1988; Braunstein et al., 1988; Morikis et al., 1989).

Previous work has shown that ligand binding kinetics in myoglobin can be modulated by varying pH, and increased

†This work was supported by grants from NSF (87-16382) and NIH (AM-35090).

0006-2960/91/0430-1237$02.50/0

CO binding rates below neutral pH have been attributed variously to distal effects involving the interaction of the bound ligand with the E7 histidine (Doster et al., 1982) or to proximal effects involving the rupture of the bond between the heme iron and the F8 histidine (Giacometti et al., 1977, 1981; Coletta et al., 1985; Traylor et al., 1983). The proximal effects are thought to arise from the presence of four-coordinate hemes in which the iron is in the heme plane and the binding activation barrier is significantly reduced. Such effects are suggested by model compound studies, where protonation of the histidine ligand at low pH leads to rupture of the iron–histidine bond and enhanced CO binding rates (Geibel et al., 1975; Cannon et al., 1976; White et al., 1979).

It is clear that an accurate understanding of pH-dependent kinetic effects requires a careful study of acid-induced structural changes. In the preceding paper (Sage et al., 1991), we used static spectroscopic measurements to characterize structural changes at the heme site due to the global conformational rearrangement of the protein that occurs below pH 4. In addition, we determined that the partially unfolded myoglobin conformation that is dominant below pH 4 is clearly distinct from the "open pocket" conformation that has been observed in MbCO[1] above pH 4 (Morikis et al., 1989). Both of these conformations are expected to differ kinetically from the "closed pocket" native conformation that is predominantly populated at neutral pH. Previous work has explored the ligand binding kinetics of different folded conformations above pH 4 (Doster et al., 1982; Ansari et al., 1987).

Here, we present a preliminary kinetic characterization of the partially unfolded state observed below pH 4. Since very fast rebinding kinetics are expected for four-coordinate hemes, proximal ligation is a key issue. Although the iron–histidine bond is clearly broken for deoxyMb *in equilibrium* (Sage et al., 1991), photolysis of MbCO above pH 2.4 produces a five-coordinate species with this bond intact. Furthermore, this species remains stable on the time scale of CO rebinding. Under extended illumination, the iron–histidine stretching mode disappears from the resonance Raman spectrum of the photoproduct, but the iron remains five-coordinate. Complete photolysis of MbCO is prevented due to rapid (subnanosecond) geminate CO recombination. In order to explain this fast rebinding phase, we propose the existence of a minority population of four-coordinate hemes in rapid exchange with the observed majority populations of five-coordinate photoproducts. We present a model that describes the complex ligation kinetics observed and point out some pitfalls that should be avoided in interpreting kinetic data in the pH < 4 region.

Theoretical Background

On the basis of the results reported in the preceding paper (Sage et al., 1991), we present a simple framework for interpreting myoglobin structure and heme ligation states at low pH. In Figure 1 we expand the standard three-state model used to describe binding and photolysis of exogenous ligands in myoglobin (Murray et al., 1988). In this model, the labels A, B, and C stand for the various states of the ligand with respect to the protein:

$$A \underset{k_{BA}}{\overset{k_L}{\rightleftharpoons}} B \underset{k_{in}}{\overset{k_{out}}{\rightleftharpoons}} C \qquad (1)$$

where A indicates CO bound to the heme, B indicates CO in the heme pocket, and C represents Mb with CO in solution.

[1] Abbreviations: Mb, sperm whale myoglobin; Fe–His, iron–histidine; cw, continuous wave; RR, resonance Raman.

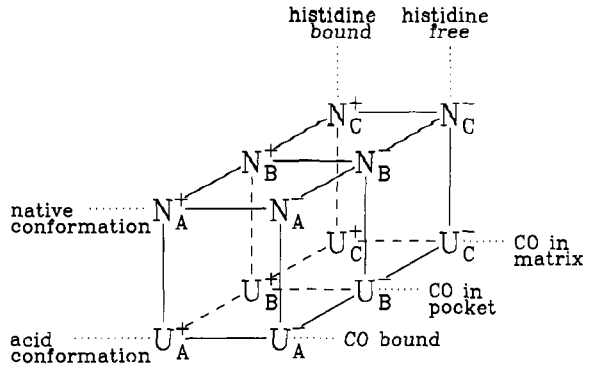

FIGURE 1: Scheme used for describing myoglobin structure and dynamics as a function of pH. A, B, and C represent the protein with CO bound to the heme, with CO in the heme pocket but not directly bound, and without CO in the heme pocket, respectively. N and U represent the global state of the protein in the native and acid conformations, respectively, and + and − indicate the presence or absence of the bond between the heme and the proximal histidine.

The various rate constants involve photolysis (k_L, where the spontaneous off rate is neglected), binding from the pocket to the heme (k_{BA}), as well as the entry (k_{in}) and exit (k_{out}) rates of the ligand between the solution and the pocket. Note that the bimolecular aspect of the problem is carried by the CO concentration dependence of $k_{in} = k'_{in}[CO]$ and that the protein concentration is assumed to be much less than [CO] so that k_{in} is constant.

One should also keep in mind that this simple model ignores intermediate states that have negligible populations in room temperature solutions and that the state denoted B here should not necessarily be interpreted as the (contact pair) B state observed in low-temperature geminate rebinding studies. The geminate states B (contact pair) and C (separated pair) observed at room temperature by Jongeward et al. (1988a) with ligands other than CO have been collapsed into a single geminate state, B, in the present simplified analysis. It should be recognized that the geminate rebinding rate, k_{BA}, observed (Henry et al., 1983) for MbCO at room temperature is quite likely the product of the binding yield from the contact pair and the rate of contact pair formation from the separated pair. Since the overall amplitude of the geminate process in MbCO is only 4%, the amplitude for the direct decay of the contact pair is much too small to be detected and the three-state model is sufficient to describe all kinetic observables in the MbCO system at neutral pH (Henry et al., 1983). As the pH is lowered and the rebinding rate from the contact pair is sufficiently increased, the amplitude for the direct decay from the contact pair should be detectable as an "unphotolyzed" fraction, with rebinding rates comparable to the laser photolysis rate. In the low-pH regime, the effective three-state analysis is still useful, bearing in mind that the states A, B, and C may need to be reinterpreted in line with the analysis of Jongeward et al. (1988a).

The generalization of the three-state model in Figure 1 is based on the structural characterization of myoglobin at low pH (Sage et al., 1991), which indicates that a complete understanding of ligand binding kinetics must allow for loss of the proximal histidine (+ = histidine present, − = histidine absent) as well as a partial loss of tertiary structure (N = native structure, U = "unfolded" structure). As might be expected, these pH-induced changes can profoundly affect the various rate constants in eq 1.

At this stage, we digress briefly in order to clarify the meaning of Figure 1 in the context of previous work performed in the intermediate and physiological pH regime (4.5–7.0).

Within this intermediate pH regime, we find that it is sufficient to consider only the states N_A^+, N_B^+, and N_C^+, since the other states in Figure 1 are not significantly populated. It is important to realize that each of the states N_A^+, N_B^+, and N_C^+ are themselves composed of numerous substates with different protein conformations (Ansari et al., 1985). These different protein substates affect the iron–porphyrin equilibrium displacement and the local conformation of the distal pocket. For example, the open and closed forms of MbCO referred to earlier (Morikis et al., 1989) are both associated with the N_A^+ state and have been identified with the A_0 and A_1 CO conformers observed by using the infrared (Ansari et al., 1987) and Raman (Morikis et al., 1989) marker frequencies of the FeCO moiety. The open conformation probably lies on the pathway toward the unfolded structure; nevertheless, its true significance at physiological pH may be related to the ability of ligands to gain access to the heme binding site. The pH dependence of the A_0 and A_1 state populations suggests that the system is primarily in an open conformation below pH 4.5. Thus, for the purpose of the low-pH analysis presented here (i.e., pH < 4.5), we denote N_A^+ as a single "state". In principle this is an oversimplification, since all states should be considered simultaneously. However, given the complexity of the problem, we believe it is reasonable to separate the analysis into low-pH (<4.5) and intermediate-pH (4.5–7.0) regimes, and consider only the "important" states within each regime.

Below pH 4, the heme ligation states observed in equilibrium are U_A^+ and U_C^-, and a discussion of ligand binding kinetics must consider all of the states in the lower half-plane of Figure 1. It is important to keep in mind that each of the U states may also be composed of numerous substates. For example, U_A^+ may share some of the properties of the A_0 substate of N_A^+ (e.g., reduced steric hindrance from the distal pocket), but have different values for k_{in} and k_{out}. Similarly, the U^- states are likely to be composed of different structures having (for example) various distances between the proximal histidine and the heme. In the discussion to be presented here, we will also be led to consider U^- substates in which an alternate ligand, possibly a solvent water, replaces the proximal histidine. Both distal and proximal ligation kinetics will vary among these different substates.

It is worth pointing out that relative time scales play a crucial role in the analysis of the various kinetic events that take place in these systems. For example, at ambient temperature in the physiological pH regime, the protein interconversions between the open and closed forms are observed to be rapid in comparison to the ligand binding rate (Lecomte & La Mar, 1985; Morikis, 1990). In such a situation, it is sufficient to consider "average" rates for the various binding steps:

$$\langle k \rangle = P_1 k_1 + P_0 k_0 \tag{2}$$

where k_1 and k_0 represent kinetic rate constants for the protein in the closed and open conformations with equilibrium populations given by P_1 and P_0. (P_0 is thought to be ~0.03 at pH 7; Morikis et al., 1989). If $k_0 \gg k_1$, as might be the case for the ligand entry rates (k_{in}), even the small population of open form at pH 7 can play a significant role in the binding process.

At low temperature, the average in eq 2 cannot be performed since the time scale for interconversion between the states is very slow. This leads to genuine inhomogeneities in the kinetic response. For the geminate rebinding reaction there exist at least two, separate, broad barrier height distributions describing the heme rebinding rates, k_{BA} (Doster et al., 1982). We believe that the breadth of these broad, finely grained, distributions is controlled by the proximal effects discussed earlier (Šrajer et al., 1988). The primary difference between the two distributions involves a relative shift along the energy barrier axis and may be due to the presence (closed) or absence (open) of distal histidine in the pocket (Champion, 1988, 1990).

Returning now to Figure 1 and ambient temperature, we see that similar time scale arguments must also be considered in the present analysis. For example, the low-pH transitions $U_C^+ \rightleftarrows U_C^-$ and $U_B^+ \rightleftarrows U_B^-$ are likely to involve fast exchange in the initial step, coupled with a much slower evolution of the tertiary structure in which the proximal histidine is protonated and moves farther away from the heme. Rates involved in the unfolding transition $N_C^+ \rightleftarrows U_C^+$ are highly pH-dependent and may occur on a wide range of time scales (Shen & Hermans, 1972; Kihara et al., 1982). The studies of U-state kinetics described here are carried out with myoglobin samples initially at equilibrium below pH 4 in order to avoid potential complications due to unfolding kinetics.

Another basic issue to keep in mind is that information determined for one sample state may not extrapolate to another. So, for example, the equilibrium constant associated with the loss of the proximal histidine in the deoxy states (B and C) is clearly different from that in the CO-bound state (A). This can lead to unfamilar kinetic pathways at low pH. For stopped-flow pH jump experiments, the sequence $N_C^+ \rightarrow U_C^+ \rightarrow U_C^- \rightarrow U_B^- \rightarrow U_A^- \rightarrow U_A^+$ is possible, while steady-state photolysis experiments at low pH must consider $U_A^+ \rightleftarrows U_B^+ \rightarrow U_B^- \rightarrow U_A^- \rightarrow U_A^+$ (as well as possible branching to the C states). When there is fast exchange between the deoxyMb ± states, the average geminate rate is given by

$$\langle k_{BA} \rangle = P_- k_{BA}^- + P_+ k_{BA}^+ \tag{3}$$

This rate can be strongly affected by only small populations of the four-coordinate deoxy state (P_-), since it is expected that $k_{BA}^- \gg k_{BA}^+$ due to the absence of proximal constraint (Traylor et al., 1983; Šrajer et al., 1988).

To conclude this section, we summarize the solutions to the simple kinetic scheme of eq 1 under various experimental conditions. We always consider the limiting case $k_{in} \ll k_{out}, k_{BA}$. Clearly, the kinetics at low pH are potentially much more complicated, but the relatively simple solutions to eq 1 in this limit are a useful reference point when considering much of the experimental data. The following solutions are given for ambient temperature and are valid in a fast exchange limit where the various rates can be considered as averages over the appropriate protein structural conformations. We let $N_A(t)$ [or, analogously, $U_A(t)$] represent the bound state population at time t after the initiation of the experiment. A computation of $N_A(t)$ [or $U_A(t)$] determines the primary spectroscopic observables since N_B and N_C both involve deoxy heme.

Stopped flow ($k_L = 0$, $N_C(0) = 1$, $N_A(0) = N_B(0) = 0$, $k_{in} \ll k_{out}, k_{BA}$):

$$N_A(t) = 1 - e^{-\alpha_{slow} t} \tag{4a}$$

with[2]

$$\alpha_{slow} = \left(\frac{k_{BA}}{k_{BA} + k_{out}} \right) k_{in} \tag{4b}$$

Flash photolysis ($k_L = 0$, $N_B(0) = 1$, $N_A(0) = N_C(0) = 0$, $k_{in} \ll k_{BA}, k_{out}$):

[2] The amplitudes for the fast process (rate $\alpha_{fast} = k_{BA} + k_{out}$) are given by $k_{BA} k_{in}/(k_{BA} + k_{out})^2$ for stopped-flow and $k_{BA} k_L/(k_{BA} + k_{out})^2$ for steady-state photolysis. These terms can be ignored under the conditions of the present analysis.

$$N_A(t) = 1 - \left(\frac{k_{out}}{k_{BA} + k_{out}}\right)e^{-\alpha_{slow}t} - \left(\frac{k_{BA}}{k_{BA} + k_{out}}\right)e^{-\alpha_{fast}t} \quad (5a)$$

with

$$\alpha_{slow} = \left(\frac{k_{BA}}{k_{BA} + k_{out}}\right)k_{in} \quad (5b)$$

and

$$\alpha_{fast} = k_{BA} + k_{out} \quad (5c)$$

Steady-state photolysis (cw Raman) ($k_L \neq 0$, $N_A(0) = 1$, $N_B(0) = N_C(0) = 0$, $k_L, k_{in} \ll k_{out}, k_{BA}$):

$$N_A(t) = \left(\frac{k_{out}k_L}{k_{in}k_{BA} + k_{out}k_L}\right)e^{-\alpha_{slow}t} + \left(\frac{k_{in}k_{BA}}{k_{in}k_{BA} + k_{out}k_L}\right) \quad (6a)$$

with[2]

$$\alpha_{slow} = \frac{k_{out}k_L + k_{in}k_{BA}}{k_{BA} + k_{out}} \quad (6b)$$

Transient Raman (pulsed laser) ($k_L \neq 0$, $N_A(0) = 1$, $N_B(0) = N_C(0) = 0$, $k_{in} \ll k_{out}, k_{BA}, k_L$, $k_L \gg k_{out}$):

$$N_A(t) = \frac{k_{BA}}{k_{BA} + k_L}e^{-\alpha_{slow}t} + \frac{k_L}{k_{BA} + k_L}e^{-\alpha_{fast}t} \quad (7a)$$

with

$$\alpha_{slow} = \frac{k_L}{k_L + k_{BA}}k_{out} \quad (7b)$$

and

$$\alpha_{fast} = k_L + k_{BA} \quad (7c)$$

Note that the orders of magnitude of the various rates can be estimated for sperm whale Mb at ambient temperature, pH 7, and [CO] $\simeq$ 1 mM: $k_{out} \sim 10^7$ s^{-1}, $k_{in} \sim 10^4$ s^{-1}, $k_{BA} \sim 10^5$ s^{-1}, and $k_L \sim 10^4$ s^{-1} (cw) or 10^{10} s^{-1} (pulsed). These values can, of course, change dramatically as the pH is lowered and states other than N^+ are populated in Figure 1. In particular, we expect k_{BA} to increase rapidly as the N^- and U^- states are populated. Similarly, it is likely that the U states have increased values of k_{in} and k_{out}.

Experimental Procedures

All MbCO samples were prepared as described previously (Sage et al., 1991). Raman photolysis measurements on stationary samples were conducted in standard fluorometer cuvettes. For the two-color pulsed photolysis experiments, MbCO was placed in a slowly spinning cell in order to minimize cell damage due to the intense photolysis pulse. For experiments as a function of illumination time, a cylindrical cell containing MbCO was mounted on the shaft of a stepping motor that changed the cell orientation by 2° at fixed time intervals. Raman measurements were performed with a triple monochromator and intensified diode array (Sage et al., 1991).

Several lasers were used as excitation and photolysis sources for Raman scattering experiments. Continuous wave (cw) excitation was obtained from the output of a dye laser (Coherent CR-599) pumped by an argon ion laser (Coherent I-100). An excimer laser (Lambda Physik EMG53) pumped a dye laser (Lumonics HyperDYE 300) containing either bis-MSB or Coumarin 440 to produce pulsed Raman excitation. All laser dyes were purchased from Exciton Corp. The frequency-doubled output of a YAG laser (Quantel YG580) at λ = 532 nm was used to produce sample photolysis in the two-color time-resolved Raman experiments. For single-pulse Raman measurements, the excimer was operated at 100 Hz. For the two-color time-resolved measurements, both the YAG and excimer were operated at 10 Hz. The YAG internal timing was modified to provide an electronic synchronization pulse approximately 4 μs before the output light pulse. This synchronization signal was used to trigger a digital delay generator (Stanford Research DG535), which fired the excimer after a variable delay. The time delay between photolysis (YAG) and probe (excimer-pumped dye) pulses was determined by direct observation of the attenuated light pulses, using a fast photodiode and an oscilloscope. Timing jitter was 10 ns or less. For all Raman measurements using pulsed excitation, pulse energy was limited to 50 μJ in order to avoid saturation of the optical transition. The intensity of the photolysis pulse was controlled by using a variable attenuator (Newport Corp.).

Results

A simple technique that yields useful dynamical information is to excite RR scattering from a sample of MbCO with either a cw or a pulsed laser, at a wavelength and intensity that will lead to a significant level of CO photolysis. Inspection of spectra recorded under these conditions yields information on the species present in the photoinduced steady state. In order to follow ligation kinetics, we are particularly interested in the 1300–1400-cm^{-1} region of the RR spectrum (Figure 2), where we may expect to observe strong peaks due to five-coordinate deoxyMb species (ν_4 = 1356 cm^{-1}) as well as from the bound MbCO species (ν_4 = 1374 cm^{-1}). On the basis of reported cross-section measurements, any spectral contributions at 1372 cm^{-1} due to the four-coordinate deoxyMb species observed in equilibrium at low pH should be negligible upon excitation at 427 nm, near the MbCO Soret peak (Sage et al., 1991).

Above pH 4.5, it is well-known that Soret-excited RR spectra of stationary samples of MbCO contain contributions from deoxyMb, and in fact it is possible to observe complete photolysis by using a tightly focused cw beam of moderate power. Below pH 4, we find that it is no longer possible to achieve this level of photolysis, but a prominent shoulder at 1356 cm^{-1} does indicate the presence of a substantial population of five-coordinate deoxyMb (Figure 2a). We obtain further dynamical information from RR spectra excited with a single frequency pulsed beam, which contain contributions from all species present within the ~10-ns width of the pulse. The results (Figure 2b) parallel those observed with cw excitation: complete photolysis is observed above pH 4.5, while below pH 4, the RR spectrum reveals spectral features at 1374 and 1356 cm^{-1} due to the bound species (U_A^+) and to five-coordinate reduced species (U_B^+ and U_C^+), respectively.

These observations indicate that substantial changes in CO binding kinetics occur upon the transition to the U state. In order to confirm this observation and determine whether there is any additional pH dependence that is independent of the N $\rightleftarrows$ U transition at pH 4, we monitor the level of photolysis as a function of pH. To quantify our observations, we record RR spectra of a stationary MbCO sample as a function of pH, controlling beam power and focus in order to maintain constant intensity in the scattering volume, and fit the ν_4 region to three Lorentzian bands, the two ν_4 peaks at 1356 and 1374 cm^{-1} and a minor peak containing contributions from both deoxyMb and MbCO at ~1390 cm^{-1}. The fractional spectral contribution due to five-coordinate deoxyMb under these conditions is given in terms of the peak areas as $A(1356)/[A(1356) + A(1374)]$ and is plotted as a function of pH in Figure 3a for both cw and pulsed measurements.[3] The scatter in the data

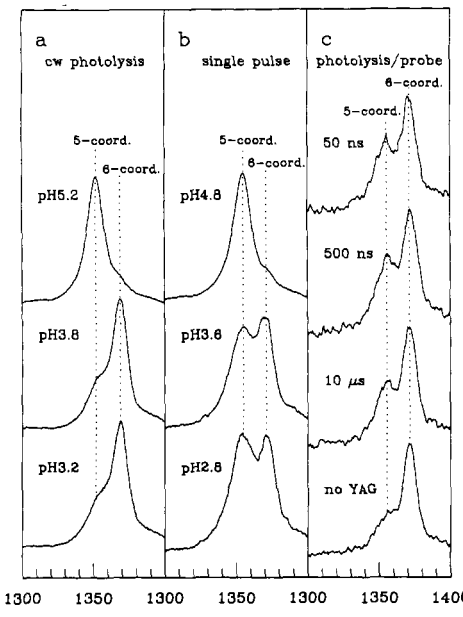

FIGURE 2: The ν_4 region of partially photolyzed MbCO under steady-state illumination (a), within the ~10-ns envelope of an intense photolyzing pulse (b), and at variable delay times following a photolysis pulse (c). Five-coordinate deoxyMb and six-coordinate MbCO species contribute strong peaks at 1356 and 1374 cm^{-1}, respectively, while four-coordinate deoxyMb species are expected to contribute only a very weak peak near 1372 cm^{-1}. The observed spectra are thus a good measure of the relative populations of five- and six-coordinate species. Below pH 4, the six-coordinate (CO-bound) fraction increases due to an enhanced geminate binding rate (a,b). Although deoxyMb has a four-coordinate heme in equilibrium below pH 4, the five-coordinate species seen on photolysis of MbCO (c) persists for at least 10 μs. The MbCO sample of (c) was at pH 3.49; other pH values are shown. All spectra were excited at 427 nm. The spectra in (a) used 60 mW of continuous wave power, while 50-μJ pulses were used to excite scattering in (b) and (c). In (a) and (b), one beam was used both to photolyze CO and to excite the scattering, while in (c), the 427-nm probe pulse used to excite the Raman spectrum followed a 15-mJ photolysis pulse produced by the frequency-doubled 532-nm output of a YAG laser. Delays between photolysis and probe pulses are given in the figure. The lower trace in (c) shows the amount of photolysis produced by the probe pulse alone. Ranges of integration times were (a) 2.5–5 min, (b) 10–17 min, and (c) 20 min.

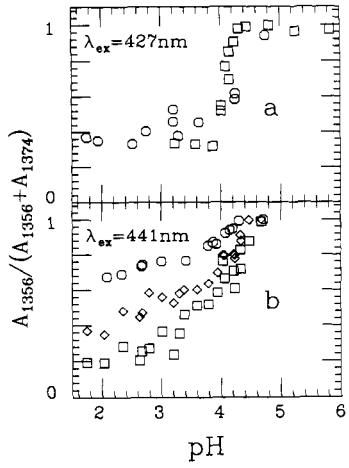

FIGURE 3: Raman photolysis titration of MbCO with pH, using the relative areas of the peaks at 1356 and 1374 cm^{-1} as a measure of fractional photolysis.[3] Data in (a) are from measurements on stationary MbCO samples using pulsed (circles) or cw (squares) 427-nm excitation. Measurements at 441-nm excitation (b) used the stepping cell apparatus described in the text. Illumination times of 10 ms (diamonds) and 1 s (squares) were used for cw measurements; for pulsed measurements, the stepping time was adjusted to 10 ms so that each pulse encountered fresh sample. In the stationary sample (a), an abrupt change in CO binding kinetics clearly occurs at pH 4.0. No other significant pH-induced kinetic variations are observed with either steady-state (squares) or pulsed (circles) photolysis. Kinetic changes below pH 4 are also apparent in (b), but the observed level is clearly a function of illumination time as well as pH. Each data set was taken with fixed power and beam focus. In continuous wave (steady-state) measurements, the laser power was fixed at 60 mW (a and b), while 50-μJ pulses at a 100-Hz repetition rate were used for the pulsed measurements. Beam focus was set so as to obtain maximum photolysis, and the integration time was typically 5 min. All samples were in 0.1 M citrate/0.2 M phosphate buffer.

from pulsed measurements is probably due to mode structure variations in the dye laser that cause small variations in the incident photon flux despite the constant pulse energy. It is clear that there is a significant change in kinetics correlated with the N → U transition at pH 4. Any further kinetic changes between pH 2 and 4 are much smaller.

The observation of a five-coordinate reduced species contributing to the spectrum of photolyzed MbCO at low pH raises the question of the time scale on which the bond to the proximal histidine ruptures to produce the four-coordinate heme observed (Sage et al., 1991) for deoxyMb in equilibrium. We have conducted two types of experiments in order to address this question. The first of these experiments follows the time dependence of the photoproduct Raman spectrum with a dual color photolysis/probe protocol. In these measurements, a λ = 532 nm pulse partially photolyzed the sample (pH 3.6) and a probe pulse (λ_{ex} = 427 nm) was used to generate the RR spectrum of the species present as a function of delay time following the photolysis pulse. The probe beam was defocused in order to minimize photolysis due to the probe pulse, which would complicate interpretation of the results, and the power of the photolysis beam was then adjusted to achieve substantial photolysis without damaging the sample cell. The results (Figure 2c) show that a significant population of the five-coordinate deoxyMb species (ν_4 = 1356 cm^{-1}) persists for at least 10 μs; i.e., the population of the five-coordinate species present at 10 μs is significantly greater than that which would be produced by probe photolysis alone. A spectrum observed 100 μs after photolysis did show a noticeable reduction in the relative intensity of the 1356-cm^{-1} band, but this is probably due to CO rebinding rather than formation of a four-coordinate species. We did not attempt to observe time dependence in the region of the iron–histidine stretching mode (ca. 220 cm^{-1}) with this dual-color protocol due to the limited amount of photolysis and the weak signal (the spectra shown in Figure 2c were recorded with ~0.5 mW average probe beam power in order to avoid saturation of the optical transition).

The dual color experiment just described is limited to observation of kinetics that occur on a time scale faster than that for ligand rebinding. In order to detect relaxation processes taking place at longer times, we have developed a novel experimental protocol using cw laser illumination (see Figure 4). The MbCO sample is mounted on the shaft of a stepping motor that periodically moves to a new position, carrying fresh,

[3] Note that the quantity plotted in Figure 3 is not in general the fractional *population* of the five-coordinate deoxy species, as the scattering cross sections of the two species are not taken into consideration. Above pH 4.5, where we believe that only two species (N_A^+ and $N_{B,C}^+$) with comparable cross sections (at λ_{ex} = 427 nm; Sage et al., 1991) are involved, the plotted quantity is approximately the fractional photolysis. Below pH 4.5, however, the cross section of the ν_4 mode is not known for the five-coordinate photoproduct, since this species clearly differs from deoxyMb at neutral pH in the 250–450-cm^{-1} region of the Raman spectrum (see Figure 5). In addition, multiple species may contribute to the intensity in the ν_4 region (see Discussion), at least in the transition region. Thus, it is not possible to calculate the fractional photolysis from the observed peak ratio even if the cross sections of these species are known.

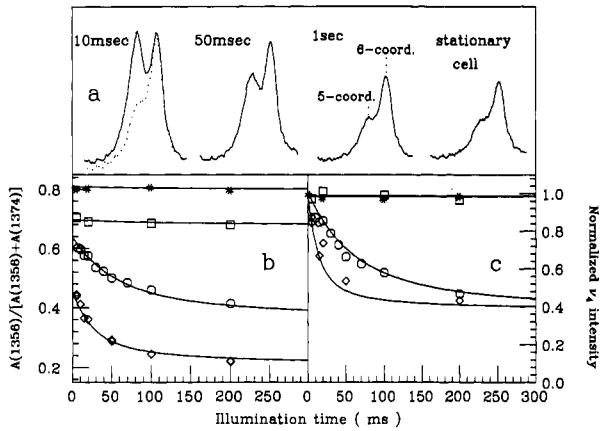

FIGURE 4: Effect of steady-state illumination on the ν_4 region of MbCO. Spectra recorded at pH 3.44 are shown in (a), while (b) and (c) contain data from samples at pH 6.98 (asterisks), pH 4.79 (squares), pH 3.44 (circles), and pH 2.41 (diamonds). For pH < 4, extended illumination produces significant changes in the relative areas of peaks due to photolyzed, five-coordinate (1356 cm^{-1}) and bound, six-coordinate (1374 cm^{-1}) heme, as can be seen by comparing the 10-ms spectrum to that observed under continuous illumination in a stationary cell [shown as the dotted trace in (a)]. The fractional area due to the 1356-cm^{-1} peak is plotted in (b) as a function of illumination time. The solid curves in (b) are fits that yield time constants of 35 ms at pH 3.44 and 9 ms at pH 2.41. The total area of both peaks also decreases as a function of illumination time, as plotted in (c). The data shown in (c) are normalized to unit intensity at zero time and fit with the same time constants used in (b). Above pH 4, no significant time dependence is observed. All spectra were gathered by using 441-nm excitation, laser power was 60 mW for pH > 4 and 210 mW for pH < 4, and integration times ranged from 2 to 6 min.

unphotolyzed material into the scattering volume under observation. The observed Raman signal then reflects the integrated populations of all species present during the time of illumination. We use illumination times that are long enough to allow steady-state populations of the A, B, and C species to be established. Relaxation processes taking place in the fraction of the sample maintained in the B and C states under steady-state illumination should lead to observable changes in the Raman spectrum as a function of illumination time. In particular, changes in heme structure or ligation are expected to affect the rates in eq 1 and thus to alter the relative intensities of the ν_4 peaks contributed by the photolyzed and bound species. Moreover, any four-coordinate heme population that is created will scatter only weakly with blue excitation, leading to a reduced overall signal intensity.

In fact, both a reduced intensity of the 1356-cm^{-1} peak relative to the 1374-cm^{-1} peak and a diminished overall scattering intensity are observed as a function of the illumination time below pH 4 (see Figure 4). Assuming a simple exponential decay, we find time constants of 35 and 9 ms at pH 3.44 and 2.41, respectively. Above pH 4.5, the peak ratio does not change under extended illumination and minimal changes are observed in the total area. Due to this dependence of the apparent photolysis level on illumination time, we repeated our pH-dependent photolysis measurements in the stepping cell. Figure 3b shows the results of these measurements for cw illumination times of 10 ms and 1 s, as well as pulsed measurements performed in the stepping cell. Note that the 441-nm excitation used in these measurements enhances the spectral contribution of the five-coordinate photoproduct. This fact causes an apparent suppression of the transition at pH 4 in the pulsed measurements, since the plotted quantity is a fractional spectral intensity rather than a fractional population.

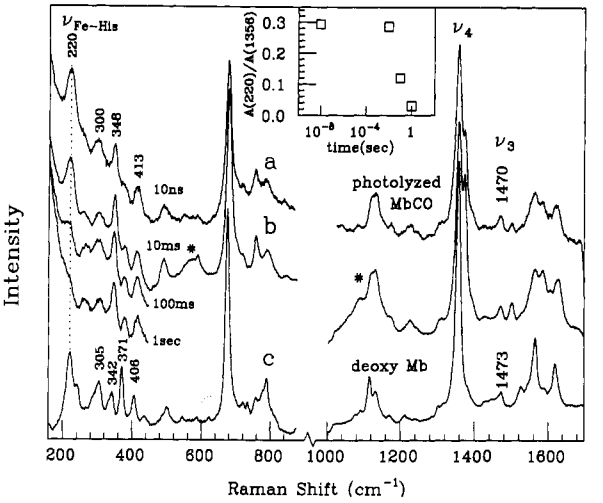

FIGURE 5: Spectral comparison of the five-coordinate deoxyMb species observed in the 10-ns transient photoproduct of MbCO at pH 3.64 (a) and produced by steady-state illumination of MbCO for variable time at pH 3.5 (b) to deoxyMb at pH 7.0 (c). Although clear differences are present at low frequencies, the iron–histidine stretching mode appears at 220 cm^{-1} in both (a) and (c), and the ν_3 and ν_4 frequencies of both spectra are characteristic of five-coordinate, high-spin ferrous hemes. The MbCO photoproduct observed under continuous illumination is also five-coordinate, but the iron–histidine mode disappears under extended illumination. Excitation was at 441 nm in all cases. The sample in (a) was mounted in a spinning cell, so that each pulse encountered fresh sample, and the spectrum was acquired by using 50-μJ pulses at a 100-Hz repetition rate. The full spectrum shown in (b) represents an average over 10 ms of steady-state illumination; additional traces of the 160–440-cm^{-1} region were recorded under 100 ms and 1 s of continuous illumination. All spectra shown in (b) were recorded by using the stepping cell apparatus described in the text with 250 mW of laser power. Emission peaks from the cw dye laser are marked with asterisks. Continuous wave excitation (power = 40 mW) was used for the neutral pH spectrum (c). Total integration times were (a) 120 min, (b) 5–10 min, and (c) 10 min.

The results shown in Figures 2 and 3 indicate that the geminate CO rebinding rate is substantially enhanced at low pH. Furthermore, the five-coordinate reduced species observed upon photolysis retains significant population at least on the time scale of ligand binding (Figure 2c) and probably longer (Figure 4). A more detailed spectroscopic characterization of the photoproduct species can lead to a better understanding of these observations. The fact that it is not possible to completely photolyze MbCO at low pH makes it more difficult to cleanly characterize the five-coordinate photoproduct. In order to minimize the contribution of unphotolyzed protein to the RR spectrum, we excite at λ_{ex} = 441 nm, which is out of resonance with the bound species (λ_{max} = 422 nm), and compare the resulting spectra with the spectrum of deoxyMb at pH 7.0. The spectrum observed with pulsed excitation (Figure 5a) contains some spectral contamination due to unphotolyzed protein (most evident in the peaks at 1372 and 1585 cm^{-1}), but we can nevertheless detect significant similarities between the five-coordinate photoproduct species at pH 3.6 (Figure 5a) and deoxyMb at pH 7.0 (Figure 5c). In addition to having ν_3 and ν_4 mode frequencies characteristic of a five-coordinate high-spin ferrous heme, it is particularly significant that the photoproduct contains a strong peak at 220 cm^{-1} corresponding to the mode assigned to Fe–His stretching in deoxyMb (Argade et al., 1984; Kitagawa et al., 1979). It is also clear, however, that the spectrum of the low-pH photoproduct exhibits some significant frequency and intensity differences relative to deoxyMb at pH 7.0 in the 250–450-cm^{-1} frequency range, which cannot be ascribed to contamination from MbCO on the basis of the observed low-pH MbCO

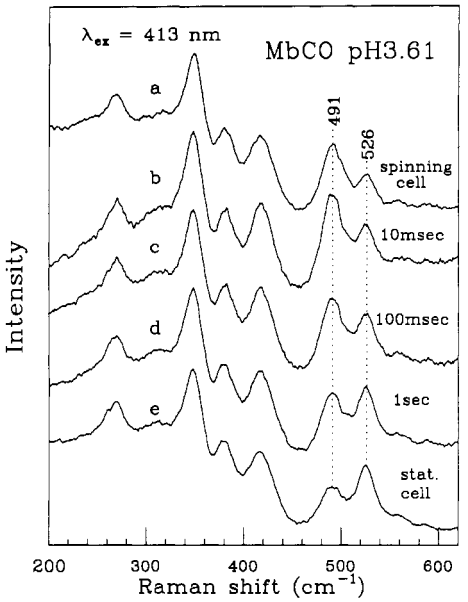

FIGURE 6: Resonance Raman spectra of MbCO at pH 3.61 in a spinning cell (a), under steady-state illumination for 10 ms (b), 100 ms (c), and 1 s (d), and under continuous illumination in a stationary cell (e). Use of the spinning cell prevents sample photolysis; thus trace (a) represents the spectrum of MbCO in equilibrium. Spectra b–e are recorded under conditions of partial photolysis, and 413-nm excitation is used in all spectra to selectively enhance scattering from the CO-bound fraction of the sample. The species that contributes the 526-cm^{-1} Fe–CO mode is a minority fraction of the sample in equilibrium (a) but its population increases as a function of illumination time (b–e) relative to the histidine-ligated MbCO species (ν_{Fe-CO} = 419 cm^{-1}) that is dominant in equilibrium. Spectra b–d were recorded by using the stepping cell apparatus described in the text. Laser power was 46 mW, and integration times were (a) 480 s and (b–e) 600 s.

spectrum (Sage et al., 1991). In particular, the modes observed at 305, 342, 371, and 406 cm^{-1} in deoxyMb at pH 7 are all believed to have contributions from bending motions of heme peripheral groups (Choi & Spiro, 1983), and it is possible that the spectral changes seen in Figure 5a are due to altered protein interactions with these groups in the low-pH photoproduct.

The analogous experiment carried out in the stepping cell apparatus at pH 3.5 with 10-ms illumination time yields a spectrum (Figure 5b) nearly identical with the transient spectrum produced with 10-ns pulses (Figure 5a), indicating that the five-coordinate photoproduct is stable on the time scale of CO binding kinetics. At longer step times, however, the iron–histidine stretching mode at 220 cm^{-1} gradually disappears. In order to establish that this observation is not simply an effect of the overall intensity loss of the spectrum at longer times (Figure 4), we measure the intensity of the 220-cm^{-1} mode relative to the 1356-cm^{-1} mode. The results (Figure 5, inset) demonstrate quantitatively that the 220-cm^{-1} mode intensity observed within 10 ns of photolysis is essentially unchanged after 10 ms of illumination but has dropped by over an order of magnitude after 1 s of illumination. Photolysis of MbCO samples prepared at pH 2.4 also produces an iron–histidine mode (with intensity reduced by a factor of 3–4) at 220 cm^{-1}, both in the 10-ns pulsed measurement and under 10 ms cw illumination.

The "bleaching" of the iron–histidine mode from the RR spectrum of the five-coordinate photoproduct suggests that the proximal ligand is replaced under extended illumination. In order to determine if similar changes take place in the CO-bound fraction, we monitor the Fe–CO stretching region of the MbCO RR spectrum, which contains a peak at 490 cm^{-1} due to the dominant histidine-ligated species as well as a peak

Scheme I

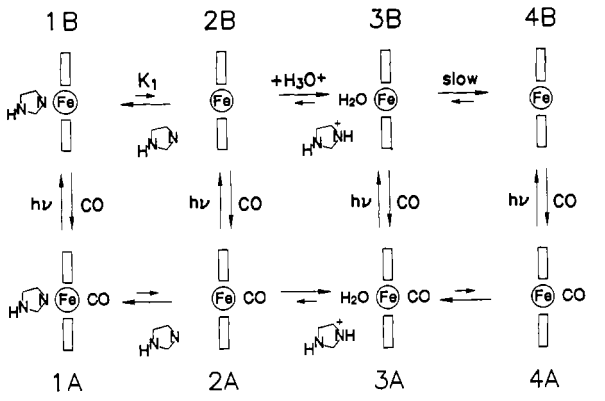

at 526 cm^{-1} contributed by a minority species in which the proximal histidine has been replaced by a weak field ligand (Sage et al., 1991). Excitation at 413 nm allows selective enhancement of the weak contribution at 526 cm^{-1}. Under extended illumination (Figure 6), a substantial increase occurs in the intensity of the 526-cm^{-1} mode relative to the 490-cm^{-1} mode that is dominant in equilibrium, indicating that alteration of the proximal ligation equilibrium occurs in the CO-bound fraction of the sample as well as in the photoproduct.

Discussion

Proximal Ligation Kinetics. Mb has been studied in depth as a model system for ligand binding to heme proteins. At low pH, the proximal ligation is clearly perturbed and is likely to account for the unusual CO binding kinetics observed. For example, very fast CO binding kinetics are expected for four-coordinate hemes, which have no proximal ligand. For MbCO, however, the majority of the hemes retain histidine ligation in the U state (Sage et al., 1991), and a key question for interpreting photolysis measurements is the time scale on which the proximal ligation state relaxes, following CO photolysis, to the four-coordinate state observed for deoxyMb in equilibrium.

The fact that the Fe–His mode is present upon photolysis (Figure 5a) and remains in the spectrum under short illumination times demonstrates that a histidine-ligated photoproduct persists on the time scale of CO rebinding. Under extended illumination, however, the histidine is replaced, as indicated by the loss of the Fe–His mode from the RR spectrum of the photoproduct (Figure 5b). The concurrent growth of the 526-cm^{-1} mode in the RR spectrum of the unphotolyzed fraction of the sample (Figure 6) also indicates a shift from dominant histidine ligation toward ligation with a weak ligand. Absorption measurements on MbCO in equilibrium suggest that the ligand may be a solvent-derived water molecule (Sage et al., 1991). Water ligation has also been suggested to occur in a transient deoxyMb species produced following a rapid pH drop (Han et al., 1990), and the RR spectrum of this species resembles that of the photoproduct produced under extended cw illumination (Figure 5b).

These observations are consistent with Scheme I. The rates and equilibria involved in Scheme I are clearly a function of protein conformation. In the N state, K_1(N) is usually assumed to be small enough that only structures 1A and 1B need to be considered in the rebinding analysis. In the U state, however, various states of proximal ligation need to be considered. In the absence of CO, a four-coordinate deoxy state, represented by 4B in Scheme I, is observed in equilibrium. Binding of CO to structure 4B leads to an equilibrium dominated by 1A, although a minority population of 3A is also observed (Sage et al., 1991). The existence of water-ligated

intermediate states was suggested by Han et al. (1990), who proposed that protonation of the proximal histidine at low pH occurs via hydronium ion insertion, leaving a water molecule coordinated to the heme. Apparently a slow protein conformational change occurs at longer times, removing both the histidine and the water ligand from the vicinity of the heme (3B → 4B). A small population of four-coordinate hemes (2B), which are rapidly exchanging with the histidine-ligated photoproduct and differ from the equilibrium structure 4B only in the proximity of the histidine to the heme, is introduced in order to account for the rapid geminate CO rebinding observed in the U state (see following section).

Under continuous illumination, the system will relax to a photostationary equilibrium in which the proximal ligation state is intermediate between the predominantly histidine-ligated state of the CO-bound state (1A) and the four-coordinate equilibrium state (4B) observed in the absence of CO. This photostationary state is controlled by the rate of CO photolysis, k_L, as all other rates in Scheme I are constants. Since the proximal ligation state relaxes slowly relative to the rate of CO photolysis and rebinding, the stepping cell experiments described above (Figures 4–6) are essentially monitoring the relaxation of the proximal ligation toward a new equilibrium state following a "k_L jump".

As noted above, Han et al. (1990) have used a nonequilibrium pH jump protocol to observe a species similar to the photoproduct (3A) seen in Figure 5b by using extended illumination. Formation of this species from native deoxyMb following a rapid drop to pH 2.6 is apparently complete within the mixing time (~6 ms). The somewhat slower relaxation rates observed here probably reflect the fact that the relaxation is taking place only during the fraction of the time that the protein is in the photolyzed state. That is, replacement of the histidine ligand by water is significantly retarded by continual cycling between the photolyzed state, which destabilizes the Fe–His bond, and the CO-bound state, in which re-formation of the bond is favored.

CO Ligation Kinetics. Comparison of the Raman photolysis measurements reported here (Figures 2–4) with eqs 6 and 7 provides information on the rates defined in eq 1. The sharp transition observed in the ratio of the ν_4 peaks below pH 4.5 (Figures 2 and 3) thus implies that at least one of the rates k_{out}, k_{in}, or k_{BA} must undergo a substantial change correlated with the transition from the N state to the U state.

On the basis of pulsed Raman photolysis measurements (Figures 2b and 3), we argue more specifically that k_{BA} is dramatically enhanced. The single-pulse RR experiments discussed here make use of 10-ns-wide 50-μJ pulses focused to a diameter of approximately 100 μm. For an extinction coefficient ϵ(427 nm) $\simeq 10^5$ cm^{-1} M^{-1} and assuming that CO is photolyzed with unity quantum yield, we then estimate that $k_L = J_L\sigma(427\text{ nm}) \simeq 5 \times 10^{10}$ s^{-1} for the duration of the pulse. Since (from eq 7c) $\alpha_{fast} \geq k_L$, the second term in eq 7a will decay in $\lesssim$20 ps and can be safely ignored. The bound population observed in the single-pulse RR experiments will then be given by the integral of the first term in eq 7a over the duration of the pulse. We cannot evaluate this integral quantitatively without knowing values for k_{out} and k_{BA} below pH 4, but it is useful to evaluate an upper limit on N_A by taking $\alpha_{slow}^{-1} \gg 10$ ns, which leads to $(1 - N_A)/N_A \geq k_L/k_{BA}$. The fact that approximately equal populations of bound and deoxy species are observed in the single-pulse RR measurements below pH 4 then implies that $k_{BA} \geq k_L \simeq 5 \times 10^{10}$ s^{-1}.

The primary motivation for studying CO rebinding at low pH is to understand the effect of proximal ligation on binding kinetics. Indeed, photolysis measurements in the "stepping cell" arrangement (Figure 4) suggest that the rebinding kinetics are a function of the ligation state. However, the RR spectrum contains contributions from species such as 3A and 3B, which have unknown scattering cross sections, preventing quantitative rate estimates. A more interesting question is whether the drastic enhancement of k_{BA} in the U state can be attributed to proximal effects. Very fast geminate rebinding to structure 3B could plausibly be attributed to replacement of the proximal histidine with the weak aquo ligand, which allows the iron to move closer to the heme plane and reduces the activation barrier for CO rebinding. However, a similar geminate rate enhancement is seen even for photolysis with a single 10-ns pulse, and it is difficult to reconcile the $\sim 10^5$ increase in k_{BA} with the observed histidine-ligated photoproduct 1B (Figure 3b and 5a).

A possible explanation of these observations is suggested by two facts:

(1) A rapidly exchanging population of four-coordinate heme, denoted as 2B in Scheme I, is expected to have a spectroscopic signature similar to the equilibrium species 4B observed in deoxyMb below pH 4. Thus, it would be spectroscopically "silent" in the pulsed RR experiments due to its very weak scattering cross section under 427-nm excitation (Sage et al., 1991) and the fact that its ν_4 peak is nearly coincident with that of the bound species. Fast rebinding pathways such as the one below would thus leave very little spectroscopic trace under our experimental conditions.

$$1A \xrightarrow{h\nu} 1B \overset{\text{fast}}{\rightleftharpoons} 2B \rightarrow 2A \rightarrow 1A$$

(2) Enhanced geminate CO binding rates are expected for four-coordinate hemes. Studies of model compounds yield observed second-order rates α_{slow} (eqs 4b and 5b) for CO binding to four-coordinate hemes that are at least an order of magnitude faster than those observed with a nitrogenous base as a fifth ligand (White et al., 1979). A large increase in CO binding rate observed for some heme model compounds at low pH has also been ascribed to loss of the nitrogenous fifth ligand due to protonation (Geibel et al., 1975; Cannon et al., 1976). Enhanced geminate rates due to a lowered activation barrier for CO binding might be expected for the planar four-coordinate heme, since a significant fraction of the activation energy encountered on ligand binding to a five-coordinate heme can be ascribed to pulling the iron into the heme plane (Coletta et al., 1985; Šrajer et al., 1988). Another factor that may affect the geminate rate is the spin state of the iron (Frauenfelder & Wolynes, 1985). Binding of CO to a four-coordinate heme involves an $S = 1 \rightarrow S = 0$ transition and is thus less spin-forbidden than binding to a five-coordinate deoxy heme ($S = 2 \rightarrow S = 0$). (In the event that the exchange is faster than the nuclear relaxation of the heme, the primary effect may involve only electronic fluctuations that influence the spin selection rules.)

The very large value for k_{BA} deduced from our low-pH pulsed photolysis measurements can thus be explained if we assume that CO photolysis leads to a rapidly exchanging mixture of two species: a relatively slowly rebinding ($k_{BA} \sim 10^6$ s^{-1}) five-coordinate majority species (1B), which is observed in the Raman spectrum of partially photolyzed MbCO (Figure 5), and a very rapidly rebinding ($k_{BA} > 10^{11}$ s^{-1}) four-coordinate minority species (2B), which cannot be observed directly with 427-nm excitation, due to its low scattering cross section. We note that rebinding of ligands other than CO to five-coordinate hemes commonly exhibits a fast process with rates in the range 10^{10}–10^{11} s^{-1} (Jongeward et al., 1988a). If we

assume that geminate CO rebinding to a four-coordinate heme occurs with a rate $k_{BA}^- \sim 10^{11}$ s^{-1}, then our rate estimate $\langle k_{BA} \rangle \sim 10^{10}$ s^{-1} implies that the fractional population of four-coordinate hemes in the photoproduct must be $P_- \sim 0.1$, according to eq 3. Due to the very large rates expected for four-coordinate hemes, it is not completely inconceivable that this "base elimination" mechanism (White et al., 1979) may be relevant even in the N state. Although K_1 may be quite small at neutral pH, the slow equilibration of heme rotational isomers observed following reconstitution of myoglobin from the apoprotein (Jue et al., 1983) demonstrates that K_1(N) is nonzero.

An alternative mechanism that could produce four-coordinate hemes in the transient photoproduct is direct photolysis of the histidine ligand in addition to CO. Picosecond absorption measurements on cytochromes (Jongeward et al., 1988b) demonstrate that endogenous heme ligands can be photodissociated but generally rebind on a picosecond time scale. More recently, a photostationary mixture of five- and six-coordinate hemes has been observed in cytochrome *c* peroxidase under cw illumination, suggesting that rebinding of the endogenous ligands may occur on significantly longer time scales if constraints are imposed by the protein conformation (Smulevich et al., 1989). If both ligands were photolyzed, it would be expected that the geminate yield for CO would depend strongly upon the relative rebinding rates of CO and histidine to the four-coordinate heme. For hemes in which the histidine ligand rebinds first, the iron will move out of the heme plane, creating a significant activation barrier for CO binding and allowing a significant fraction of the CO ligands to escape from the heme pocket. If the histidine rebinding rate is sufficiently retarded due to protein constraints, however, it may be expected that a significant fraction of the four-coordinate hemes will rebind CO on a picosecond time scale.

Some of the issues discussed above could be addressed by direct observation of the four-coordinate heme population that we have inferred from the large geminate rate. Such observations will probably be difficult to achieve by using Raman techniques, even with excitation nearer resonance with the four-coordinate species, due to the relatively small population expected for the four-coordinate heme and to the fact that many of the Raman peaks observed for this species overlap with peaks due to unphotolyzed MbCO (Sage et al., 1991). However, since the absorption band observed for the four-coordinate species is significantly blue-shifted relative to the five- and six-coordinate species likely to be observed following photolysis, time-resolved multiple-wavelength absorbance measurements will probably be an important tool for quantitative studies of the populations and binding kinetics of four-coordinate heme species.

Comments on Previous Investigations. The results presented above suggest that the primary effect of pH on CO binding kinetics is an increase in the geminate rate correlated with the sharp N → U transition at pH 4. Furthermore, there is evidence of fast geminate rates even in the presence of a histidine-ligated photoproduct. These results should be contrasted with previous interpretations of fast CO binding kinetics in Mb at low pH (Giacometti et al., 1977; Traylor et al., 1983; Coletta et al., 1985). These studies reported pH–rate profiles that were ascribed to a single-proton titration of the proximal histidine at pK = 3.45 within a native protein conformation. For these measurements, a solution of deoxyMb at neutral pH was rapidly mixed with a CO-saturated low-pH buffer, and the rate of the absorbance change as a function of time after mixing was followed at a single wavelength. The apparent discrepancy with the present results (i.e., a broad transition at pH 3.5 rather than a sharp transition at pH 4) has led us to reexamine the stopped-flow studies.

It is important to realize that the observed second-order rate, k_{obs}, is *not* a direct measure of k_{BA}, as implied by Coletta et al. (1985), Traylor et al. (1983), and Giacometti et al. (1977). It is expected that proximal histidine protonation will affect the geminate rate k_{BA}, but the rate measured by using stopped-flow techniques, $k_{obs} \equiv \alpha_{slow} = [k_{BA}/(k_{BA} + k_{out})]k_{in}$ (eq 4B), is proportional to k_{BA} only in the limit of low geminate yield (i.e., when $k_{BA} \ll k_{out}$). This limit is believed to hold for CO binding at neutral pH, where k_{BA} controls the overall binding rate (Henry et al., 1983), but k_{in} will become rate limiting for high geminate yields ($k_{BA} \gg k_{out}$) such as we observe below pH 4. Thus, the value pK = 3.45 for proximal histidine protonation derived on the basis of the assumption that $k_{obs} \propto k_{BA}$ would have to be taken as an upper limit on the actual pK in the N state of deoxyMb. Similar qualifications may apply to model compound studies (Geibel et al., 1975; Cannon et al., 1976; White et al., 1979), since CO binding must become diffusion-limited for sufficiently large values of k_{BA}. The limiting second-order rate constant reported for CO binding to sperm whale Mb at low pH ($\sim 10^7$ M^{-1} s^{-1}; Coletta et al., 1985; Traylor et al., 1983; Giacometti et al., 1977) should probably be assigned to k_{in}' for the structure (N, U, or intermediate) actually being probed in the stopped-flow experiments.

The validity of the claim (Coletta et al., 1985) that a rapid pH drop kinetically stabilizes a state in which (a) the protein maintains a native conformation and (b) protonation of the proximal histidine results in a four-coordinate heme (N_C^- in the notation of Figure 1) is a serious issue for the qualitative interpretation of stopped-flow measurements. Recent RR and absorption measurements (Han et al., 1990), which used a continuous-flow system to observe reduced Mb species formed following a rapid pH drop, raise questions about both of these assumptions. Raman results obtained in these experiments demonstrate that the heme in deoxyMb remains five-coordinate within 6 ms of a drop to pH 2.6, although the proximal histidine appears to have been displaced, possibly due to protonation. Additional structural changes in the heme environment on this time scale are also proposed by Han et al., on the basis of observations of MbCO. In fact, the reported changes in the RR spectrum of MbCO immediately following the pH drop (Han et al., 1990) are nearly identical with those reported for the histidine-ligated majority species observed in equilibrium in the U state (Sage et al., 1991), although the weak 526-cm^{-1} Fe–CO mode contributed by the minority species (3A in Scheme I) is absent at 6 ms.

The fact that spectroscopic changes characteristic of U-state MbCO in equilibrium appear within 6 ms of a drop to pH 2.6 suggests the possibility that the N → U transition may take place faster than achievable mixing times at low pH. Circular dichroism measurements of the oxidized protein following a pH drop (Kihara et al., 1982) also support this notion. Below pH 3, for instance, the entire change in the circular dichroism signal at 220 nm, which monitors the loss of α-helical content in the U state, is complete within the mixing time for metMb. Interestingly, the concurrent Soret absorbance change involves only a small red shift (2–3 nm), while the large blue shift associated with the loss of the proximal histidine occurs on a much slower time scale ($\sim$100 ms at pH 3; Shen & Hermans, 1972). These studies and those of Han et al. (1990) are consistent with rapid unfolding within the mixing time, followed by a much slower equilibration of the proximal li-

gation, at least below pH 3. Further work will be required to properly assess this hypothesis and its extension to reduced forms of the protein. Note that, on the basis of comparison with the multiple-wavelength measurements of Shen and Hermans (1972), the slow component ($k^{-1} \sim 200$ ms) observed (Coletta et al., 1985) in the transient deoxyMb absorbance following a pH drop is probably due to loss of the proximal ligand (e.g., 3B → 4B in Scheme I). Thus, the possibility that the N → U transition takes place on a more rapid time scale cannot be ruled out as assumed by Coletta et al. (1985).

The fact that more complex unfolding kinetics are observed above pH 3 (Shen & Hermans, 1972; Kihara et al., 1982) may help reconcile the broad pH–rate profile observed in stopped-flow studies of CO-binding kinetics (Coletta et al., 1985; Traylor et al., 1983; Giacometti et al., 1977) with the relatively sharp pH dependence observed in the present photolysis measurements (Figure 3a). In particular, the pH dependence observed in stopped-flow kinetics measurements, rather than being due to titration of the proximal histidine with $pK \leq 3.45$, could be attributed to pH-dependent populations of N and U and possibly intermediate structures as well. Such an explanation would be consistent with photolysis measurements of equilibrium samples reported here, since the observed pH dependence (Figure 3a) is directly correlated with the populations of the N and U states. Since we see no significant pH-dependent behavior below pH 4, the present studies suggest that the effective pK for creating fast-rebinding structures (2B and 3B) must be shifted above pH 4 in the equilibrium U state. For example, the expression for the effective pK can be approximated by $-\log(K_H/K_1)$ when K_1 is much less than unity and K_H is the usual proton-dependent equilibrium constant between structures 3B and 2B. Thus, if $K_H \simeq 10^{-6}$, as might be expected for the deligated histidine in 3B and 2B, we have $pK_{eff} \leq 3$ if $K_1(N) \leq 10^{-3}$ and $pK_{eff} \simeq 5$ if $K_1(U) = 10^{-1}$.

Regardless of whether the spectroscopic changes observed by Han et al. (1990) can be attributed to rapid unfolding, it seems likely that local structural changes in the heme vicinity, comparable to those observed upon the global N → U transition, do occur within achievable mixing times. The RR spectra of deoxyMb and MbCO observed following a drop to pH 2.6 (Han et al., 1990) resemble those of species observed in the equilibrium U-state conformation and assigned as 1A and 3B in Scheme I. Thus, it is difficult to know whether pH-dependent rate changes observed in a stopped-flow protocol should be attributed to altered heme coordination or to additional structural changes with pH. A reliable interpretation of stopped-flow measurements will thus require detailed studies to characterize both protein conformation and heme ligation throughout the pH range under study, particularly in the critical range from pH 3 to 4.

Conclusions

The data presented here and in the preceding paper (Sage et al., 1991) allow the direct correlation of structural and kinetic properties of myoglobin at low pH. The kinetics of binding both proximal and distal ligands within the U state prove to be surprisingly complex. The transition to the U state at low pH is correlated with the appearance of a subnanosecond geminate CO rebinding phase, which we attribute to a small population of four-coordinate hemes (2B) in rapid exchange with the dominant histidine-coordinated photoproduct (1B). Using a novel technique, we have also succeeded in observing a proximal ligation change in the deoxy heme that occurs slowly relative to CO rebinding. A complete understanding of myoglobin ligation kinetics in this pH region involves consideration of a minimum of four deoxy states, as outlined in Scheme I. Further measurements of ligation kinetics below pH 4 will require consideration of these complexities. The presence of multiple spectroscopic species, for instance, leads to ambiguities in the interpretation of absorbance decay curves recorded at a single wavelength. Moreover, the interpretation of experiments such as RR or multiple-pulse transient absorbance measurements, which involve extended illumination of a stationary sample of MbCO at low pH, requires careful structural characterization that takes into account the fact that the proximal ligation of the heme is likely to be time-dependent.

Registry No. CO, 630-08-0; histidine, 71-00-1; iron, 7439-89-6; heme, 14875-96-8.

References

Ansari, A., Berendzen, J., Bowne, S. F., Frauenfelder, H., Iben, I. E. T., Sauke, T. B., Shyamsunder, E., & Young, R. D. (1985) *Proc. Natl. Acad. Sci. USA 82*, 5000.

Ansari, A., Berendzen, J., Braunstein, D., Cowen, B. R., Frauenfelder, H., Hong, M. K., Iben, I. E. T., Johnson, J. B., Ormos, P., Sauke, T. B., Scholl, R., Schulte, A., Steinbach, P. J., Vittitow, J., & Young, R. D. (1987) *Biophys. Chem. 26*, 337.

Argade, P. V., Sassaroli, M., Rousseau, D. L., Inubushi, T., Ikeda-Saito, M., & Lapidot, A. (1984) *J. Am. Chem. Soc. 106*, 6593–6596.

Braunstein, D., Ansari, A., Berendzen, J., Cowen, B. R., Egeberg, K., Frauenfelder, H., Hong, M. K., Ormos, P., Sauke, T. B., Scholl, R., Schulte, A., Sligar, S. G., Springer, B. A., Steinbach, P. J., & Young, R. D. (1988) *Proc. Natl. Acad. Sci. U.S.A. 85*, 8497–8501.

Cannon, J., Geibel, J., Whipple, M., & Traylor, T. G. (1976) *J. Am. Chem. Soc. 98*, 3395–3396.

Champion, P. M. (1988) in *Proceedings of the International Symposium on Frontiers in Science*, American Institute of Physics Conference Proceedings No. 180 (Chan, S. S., & Debrunner, P. G., Eds.) pp 310–324, American Institute of Physics, New York.

Champion, P. M. (1989) in *Protein Structure and Engineering* (Jardetzky, O., Ed.) pp 347–354, Plenum, New York.

Choi, S., & Spiro, T. G. (1983) *J. Am. Chem. Soc. 105*, 3683–3692.

Coletta, M., Ascenzi, P., Traylor, T. G., & Brunori, M. (1985) *J. Biol. Chem. 260*, 4151–4155.

Doster, W., Beece, D., Bowne, S. F., DiIorio, E. E., Eisenstein, L., Frauenfelder, H., Reinisch, L., Shyamsunder, E., Winterhalter, K. H., & Yue, K. T. (1982) *Biochemistry 21*, 4831–4838.

Frauenfelder, H., & Wolynes, P. G. (1985) *Science 229*, 337.

Geibel, J., Chang, C. K., & Traylor, T. G. (1975) *J. Am. Chem. Soc. 98*, 5924–5926.

Giacometti, G. M., Traylor, T. G., Ascenzi, P., Brunori, M., & Antonini, E. (1977) *J. Biol. Chem. 252*, 7447–7448.

Giacometti, G. M., Ascenzi, P., Bolognesi, M., & Brunori, M. (1981) *J. Mol. Biol. 146*, 363–374.

Han, S. H., Rousseau, D. L., Giacometti, G., & Brunori, M. (1990) *Proc. Natl. Acad. Sci. U.S.A. 87*, 205–209.

Henry, E. R., Sommer, J. H., Hofrichter, J., & Eaton, W. A. (1983) *J. Mol. Biol. 166*, 443–451.

Jongeward, K. A., Magde, D., Taube, D. J., Marsters, J. C., Traylor, T. G., & Sharma, V. S. (1988a) *J. Am. Chem. Soc. 110*, 380–387.

Jongeward, K. A., Magde, D., Taube, D. J., & Traylor, T. (1988b) *J. Biol. Chem. 263*, 6027.

Jue, T., Krishnamoorthi, R., & La Mar, G. N. (1983) *J. Am. Chem. Soc. 105*, 5701–5703.

Kihara, T., Takashi, E., Yamamura, K., & Tabushi, I. (1982) *Biochim. Biophys. Acta 702*, 249–253.
Kitagawa, T., Nagai, K., & Tsubaki, M. (1979) *FEBS Lett. 104*, 376–378.
Lecomte, J. T. J., & La Mar, G. N. (1985) *Biochemistry 24*, 7388–7395.
Morikis, D. (1990) Ph.D. Thesis, Northeastern University, Boston, MA.
Morikis, D., Champion, P. M., Springer, B. A., & Sligar, S. G. (1989) *Biochemistry 28*, 4791–4800.
Moffat, K., Deatherage, J. R., & Seyberg, D. W. (1979) *Science 206*, 1035–1042.
Murray, L., Hofrichter, J., Henry, E., & Eaton, W. (1988) *Biophys. Chem. 29*, 63–76.
Nagai, K., Luisi, B., Shih, D., Miyazaki, G., Imai, K., Poyart, C., De Young, A., Kwiatkowski, L., Noble, R. W., Lin, S.-H., & Yu, N.-T. (1987) *Nature 329*, 858.
Olson, J. S., Mathews, A. J., Rohlfs, R. J., Springer, B. A., Egeberg, K. D., Sligar, S. G., Tame, J., Renaud, J.-P., & Nagai, K. (1989) *Nature 336*, 265–266.
Puett, D. (1973) *J. Biol. Chem. 248*, 4623–4634.
Sage, J. T., Morikis, D., & Champion, P. M. (1991) *Biochemistry* (preceding paper in this issue).
Shen, L. L., & Hermans, J., Jr. (1972) *Biochemistry 11*, 1836–1849.
Smulevich, G., Miller, M. A., Gosztola, D., & Spiro, T. G. (1989) *Biochemistry 28*, 9905–9908.
Šrajer, V., Reinisch, L., & Champion, P. M. (1988) *J. Am. Chem. Soc. 110*, 6656–6670.
Traylor, T. G., Dearduff, L. A., Coletta, M., Ascenzi, P., Antonini, E., & Brunori, M. (1983) *J. Biol. Chem. 258*, 12147–12148.
White, D. K., Cannon, J. B., & Traylor, T. G. (1979) *J. Am. Chem. Soc. 101*, 2443–2454.

Two-Dimensional NMR and Structure Determination of Salmon Calcitonin in Methanol†

Robert P. Meadows,‡ Edward P. Nikonowicz,‡ Claude R. Jones,‡ James W. Bastian,§ and David G. Gorenstein*,‡

Department of Chemistry, Purdue University, West Lafayette, Indiana 47907, and 126 Chestnut Street, Park Forest, Illinois 60466

Received August 9, 1990; Revised Manuscript Received October 25, 1990

ABSTRACT: The structure of the 32-residue peptide salmon calcitonin (sCT) in 90% MeOH–10% H_2O has been investigated by two-dimensional NMR techniques and molecular modeling. Sequential assignments for nearly all of the 32 spin systems have been obtained, and results indicate that the heptaresidue loop formed by the disulfide bond between Cys-1 and Cys-7 is followed by an α-helical segment from Val-8 through Tyr-22. A region of conformational heterogeneity is observed for residues 20–25, resulting from the slow isomerism of the cis and trans forms of Pro-23. The C-terminal segment is found to exist in an extended conformation.

Salmon calcitonin I (sCT) is a 32 amino acid peptide which is physiologically important for inhibiting activity of osteoclasts (Niall et al., 1969; Kallio et al., 1972). It is administered by daily injection for the treatment of osteoporosis (Wallach et al., 1977), Pagets disease (Avramides et al., 1974), hypercalcemia (Hosking & Weller, 1986), and reflex sympathetic dystrophy (Gobelet, 1986). Known forms of calcitonin include those produced by the parafollicular cells of the thyroid (human, rat, pig, sheep, and cow) and those from the ultimobranchial glands of salmon (I, II, and III), eel, and chicken (Potts et al., 1972; Azria, 1989). Ultimobranchial calcitonins, tested in mammals, are approximately 30-fold more potent than calcitonins of thyroidal origin, yet all are 32 amino acids in length having an amino-terminal 1–7 disulfide bridge and a carboxyl-terminal proline amide (Azria, 1989). The primary sequence of sCT is shown in Figure 1.

Information on the conformation of calcitonin in the presence of its receptor should permit design of analogues having fewer side effects and better absorbability when given by noninjectable routes. Epand et al., using circular dichroism, have shown the amphiphilic sCT to have little secondary structure in water but to exhibit significant α-helix in the presence of dimyristoylphosphatidylglycerol (DMPG) or 90% MeOH/10% water (Epand et al., 1983; Orlowski et al., 1987). NMR investigations of other membrane-active peptides, in particular the studies of δ-hemolysin, have shown that there may be little difference in structures produced in methanolic solvents and those resulting from the more complicated lipid micellar environments (Inagaki et al., 1989). Thus, our initial investigations into the conformation of sCT were performed in 90% MeOH in the expectation that the results may have relevance to that of the conformation of calcitonin in the presence of its lipid-bound receptor.

Materials and Methods

Calcitonin was prepared by solid-phase chemistry, was purified by preparative HPLC, and was the generous gift of Armour Pharmaceutical, Kankakee, IL. NMR samples were prepared by dissolving the lyophilized sCT peptide in ~650

† Supported by the NIH (A127744), the Purdue University Biochemical Magnetic Resonance Laboratory which is supported by the National AIDS Research Center at Purdue (AI7277713), and the NSF Biological Facilities Center on Biomolecular NMR, Structure and Design at Purdue (BBS 8614177 and DIR-9000360).

‡ Purdue University.
§ Park Forest, IL.

0006-2960/91/0430-1247$02.50/0